Adenosine 5′-Diphosphate Binding and the Active Site of Nucleoside Diphosphate Kinase†,‡

Solange Moréra,§ Ioan Lascu,‖ Christian Dumas,§,⊥ Gérard LeBras,§ Pierre Briozzo,§ Michel Véron,‖ and Joël Janin*,§

Laboratoire de Biologie Structurale, UMR 9920 CNRS-Université Paris-Sud, Bât. 34, 1 Avenue de la Terrasse, 91198 Gif-sur-Yvette, France, and Unité de Biochimie Cellulaire, CNRS-URA 1129, Institut Pasteur, 75724 Paris Cedex 15, France

Received July 19, 1993; Revised Manuscript Received September 29, 1993⊛

ABSTRACT: The X-ray structure of nucleoside diphosphate kinase (NDP kinase) from the slime mold *Dictyostelium discoideum* has been determined to 2.2-Å resolution and refined to an *R*-factor of 0.19 with and without bound ADP–Mg^{2+}. The nucleotide binds near His 122, a residue which becomes phosphorylated during the catalytic cycle. The mode of binding is different from that observed in other phosphokinases, and it involves no glycine-rich sequence. The adenine base makes only nonpolar contacts with the protein. It points outside, explaining the lack of specificity of NDP kinase toward the base. The ribose 2′- and 3′-hydroxyls and the pyrophosphate moiety are H-bonded to polar side chains. A Mg^{2+} ion bridges the α- to the β-phosphate which approaches the imidazole group of His 122 from the Nδ side. The geometry at the active site in the ADP–Mg^{2+} complex suggests a mechanism for catalysis whereby the γ-phosphate of a nucleoside triphosphate can be transferred onto His 122 with a minimum of atomic motion.

Nucleoside diphosphate kinase (NDP kinase) exchanges γ-phosphates between nucleoside tri- and diphosphates through a phosphohistidine intermediate:

$$XTP + E \leftrightarrow XDP + E\text{–}P$$

$$E\text{–}P + YDP \leftrightarrow E + YTP \quad (1)$$

The enzyme is found in all cells, shows little specificity toward the X and Y bases, and accepts nucleotides and deoxynucleotides as substrates. The phosphate transfer is very efficient, with turnover numbers larger than $10^3\ s^{-1}$ (Parks & Agarwal, 1973; Gilles et al., 1991). In recent years, NDP kinase gene sequences have become available from a number of eukaryotic and bacterial sources. All code for chains of about 150 residues (M_r about 17 000) with a high degree of sequence homology, especially among eukaryotes (Rosengard et al., 1989; Shimada et al., 1993).

The first three-dimensional structure of a NDP kinase to be reported was for a point mutant of the protein from the slime mold *Dictyostelium discoideum*. The 2.2-Å X-ray structure solved by Dumas et al. (1992) shows the protein to be a symmetrical hexamer. The subunit fold, novel for a kinase, does not contain the classical mononucleotide binding fold (Schulz, 1986, 1992) found in the $p21^{ras}$ oncogene protein and in adenylate kinase, two phosphate-transfer enzymes of comparable size to the NDP kinase subunit. Instead, NDP kinase is built around a four-stranded antiparallel β-sheet with α-helical connections. Its topology is the same as in *Pseudomonas aerogenes* ferredoxin (Adman et al., 1973) and in the allosteric domain of *Escherichia coli* aspartate carbamoyltransferase (ATCase). The allosteric domain binds effectors ATP and CTP, two substrates of NDP kinase. Their mode of binding to the allosteric domain being known (Gouaux et al., 1990), a plausible location of the NDP kinase active site was suggested by analogy. It fitted with the observed location of residue 122, which is the phosphorylated histidine in *Dictyostelium* NDP kinase. This residue was substituted with a cysteine in the H122C mutant protein studied by Dumas et al. (1992). The mutant protein has no enzymic activity, and no functional studies could be performed.

We report here the X-ray structure of the wild-type *Dictyostelium* enzyme and that of its complex with ADP–Mg^{2+}. They are closely similar to each other and to the H122C mutant protein. ADP binds near His 122 as expected, but not like ATP in ATCase. The adenine base is in a cleft near the protein surface and makes only nonpolar interactions. In contrast, the ribose and pyrophosphate moieties make polar interactions with side chains of conserved residues. The geometry of the active site in the ADP–Mg^{2+} complex suggests a mechanism for the transfer of a γ-phosphate onto the imidazole group of His 122.

MATERIALS AND METHODS

Protein Preparation, Crystallization, and Data Collection. The cloned *gip* gene from *Dictyostelium* (Lacombe et al., 1990) was expressed in *E. coli*, and active NDP kinase was purified as described (Wallet et al., 1990) by negative adsorption on a DEAE Sephacel column at pH 8.6 and affinity chromatography on Blue Sepharose at pH 7.4. Elution with 1.5 mM ATP yielded pure protein, as could be checked by SDS–PAGE. We used seleniated protein (Hendrickson et al., 1990) in early crystallographic experiments. It was prepared by growing an *E. coli* methionine auxotroph on selenomethionine (Sigma). It had full enzymic activity and could be purified and crystallized under the same condition as normal NDP kinase.

Crystallization of wild-type *Dictyostelium* NDP kinase in 2.0 M ammonium sulfate yields the hexagonal crystal form

† This work was supported in part by funds from ARC, Comité de Paris de la Ligue Nationale Française contre le Cancer, INSERM (CRE 920113), and Agence Nationale de Recherche contre le SIDA and by a stipend to S.M. from IFSBM (Villejuif).

‡ Coordinates have been deposited in the Protein Data Bank under file names 1NDK and 2NDK.

* Corresponding author (telephone, 33.1.69 72 34 77; fax, 33.1.69 82 31 29; E-mail, janin@lure.ups.circe.fr).

§ Laboratoire de Biologie Structurale.

‖ Unité de Biochimie Cellulaire.

⊥ Present address: CRBM-CNRS BP 5051, Route de Mende, 34033 Montpellier, France.

⊛ Abstract published in *Advance ACS Abstracts*, December 15, 1993.

0006-2960/94/0433-459$04.50/0

Table 1: Crystal Forms of Wild-Type *Dictyostelium* NDP Kinase

	form I	form II	form III
precipitant	ammonium sulfate	PEG 6000	PEG 6000
ligand			ADP–Mg^{2+}
space group	$P6_322$	$P6_322$	$R3$
cell parameters[a]			
$a = b$ (Å)	75.3	74.6	73.2
c (Å)	211.0	105.5	158.5
asymmetric unit			
volume (Å^3)	86300	41200	81400
protein content	dimer	monomer	dimer

[a] Hexagonal lattice with $\alpha = \beta = 90°$ and $\gamma = 120°$.

Table 2: Statistics on Crystallographic Analysis

	form I	form II	form III
diffraction data			
resolution (Å)	2.4	2.2	2.2
measured intensities	82302	48114	31166
unique reflections	13703	8780	15408
completeness (%)	93	90	88
R_{merge} (%)[a]	5.6	3.5	7.4
refinement			
R_{cryst} (%)[b]	22	19	19
reflections	5365	8689	15348
protein atoms	1131	1131	2284
nucleotide atoms			56
solvent atoms	16	92	157
av B (Å^2)	23.8	18.8	17.1
geometry (Å)[c]			
bond lengths (1–2) [0.02]	0.015	0.015	0.014
bond angles (1–3) [0.04]	0.048	0.037	0.044
planar groups (1–4) [0.05]		0.047	0.050
planarity [0.01]		0.014	0.010

[a] $R_{merge} = \sum|I(h)_i - \langle I(h)\rangle|/\sum\langle I(h)\rangle$. [b] $R_{cryst} = \sum||F_o| - |F_c||/\sum|F_o|$, calculated with PROLSQ on all reflections for forms II and III and on even-l reflections only for form I. The 2.2–2.3-Å shell has $R = 0.24$ and 0.25 in forms II and III. [c] Statistics from PROLSQ. Target RMS deviations are in brackets.

I with two 17-kDa subunits in their asymmetric unit (Dumas et al., 1991). The H122C mutant protein also crystallizes in this precipitant. It yields form II crystals, which belong to the same space group, $P6_322$, as form I but have a shorter c axis and only one subunit per asymmetric unit (Dumas et al., 1992). For reasons discussed below, form I crystals grown in ammonium sulfate proved unsuitable for high-resolution studies. We therefore turned to other precipitants and eventually obtained well-diffracting form II crystals with the wild-type protein. They grow in hanging drops containing 5% PEG 6000 (Sigma), 20 mM $MgCl_2$, and 50 mM Tris-HCl buffer, pH 8.0, over pits containing 10% PEG 6000 in the same buffer. Addition of 10 mM ADP led to the appearance of crystals with a different habit, defining crystal form III. They grow over pits containing 17.5% PEG 6000, belong to space group $R3$, and have a dimer in their asymmetric unit (Table 1).

All diffraction data were collected on crystals kept at 4 °C on the W32 station at the LURE-DCI synchrotron radiation center (Orsay, France) with a photosensitive plate system and monochromatic 0.91-Å X-rays. Only one crystal of each form was required. With form I, 75° of rotation about c were recorded at the rate of 1 deg per minute of exposure and per image. The particular crystal for which statistics are given in Table 2 was of the seleniated protein. With form II, 60° was recorded at the same rate about c; with form III, 90° was recorded about an arbitrary axis of rotation. Intensities were evaluated with the program MOSFLM as adapted for the image plate system (Leslie et al., 1986). Further processing used the CCP4 program suite (CCP4, Daresbury Laboratory, Warrington, U.K.). Electron density maps ($2F_o - F_c$ or $F_o - F_c$) were examined with FRODO (Jones, 1985). Crystallographic refinement was performed with the conjugate-gradient facility of X-PLOR (Brünger et al., 1987). PROLSQ (Hendrickson, 1985) was used near the end of refinement and for statistics.

Crystal Structure Solution. NDP kinase structures described here derive from the model of the H122C protein in form II crystals (Dumas et al., 1992). The mutant structure was solved by single isomorphous replacement with Hg^{2+} at the engineered cysteine and refined to an R-factor of 0.203 against data to 2.2-Å resolution. Hexagonal form I is very similar to form II, but the c axis is twice as long, so that $hk2l$ Bragg reflections are equivalent to hkl reflections in form II. At a resolution less than 5 Å, reflections with odd-l indices are weak in form I, and intensities of even-l reflections are highly correlated to those in form II. This observation showed that the molecular packing is the same in the two hexagonal forms. An electron density map was calculated using only even-l reflections and phases derived from the H122C model. When data collected on seleniated protein were used, high density was observed at expected positions in the Met 80 and Met 94 side chains, showing that selenium was present and that the phases were approximately correct. Moreover, the histidine side chain replacing Cys 122 was clearly visible in the map. After the necessary changes were made, X-PLOR refinement done on even-l reflections only eventually dropped the R-factor to 0.22 at 2.6-Å resolution with very little change in the structure (Table 2).

Whereas these results implied that the wild-type protein has essentially the same structure as the H122C mutant in ammonium sulfate, the study of form I was abandoned when diffraction data on PEG-grown crystals became available. Form II crystals of wild-type NDP kinase diffract to beyond 2-Å resolution and are nearly isomorphous to crystals of the H122C mutant. Conjugate-gradient refinement with X-PLOR of the H122C model against these data quickly dropped the R-factor to 0.25 at 2.8-Å resolution. When the electron density map was examined, only minor modifications of the model were required except for the substitution at residue 122. As in the H122C structure, N-terminal residues 2–7 had no density and are missing from the final model. After addition of 92 water molecules, further refinement with X-PLOR and PROLSQ reduced the R-factor to the present 0.19 against essentially all measured reflections at 2.2-Å resolution.

Form III crystals belong to space group $R3$. Molecular replacement from the hexagonal forms was straightforward. The volume of the rhombic primitive cell indicates that it contains an hexamer. Then, its 3-fold axis must be the c axis of the nonprimitive hexagonal lattice, with the molecular 2-fold axes in the (a, b) plane. A self-rotation function located the 2-fold axes 12° off their orientation in form I. This was confirmed by placing the H122C hexamer at the cell origin, rotating it by 12° about c, and calculating an R-factor of 0.38 against form III data at 2.6-Å resolution. An electron density map calculated with phases from the rotated H122C model showed the His 122 side chain and, next to it, density that could be interpreted as bound ADP. The interpretation became unambiguous after a few cycles of conjugate-gradient refinement, so that the nucleotide could be built in density and the model of the complex subjected to further refinement. ADP density from an omit map is shown in Figure 1. The present model contains a dimer with bound ADP, Mg^{2+}, and

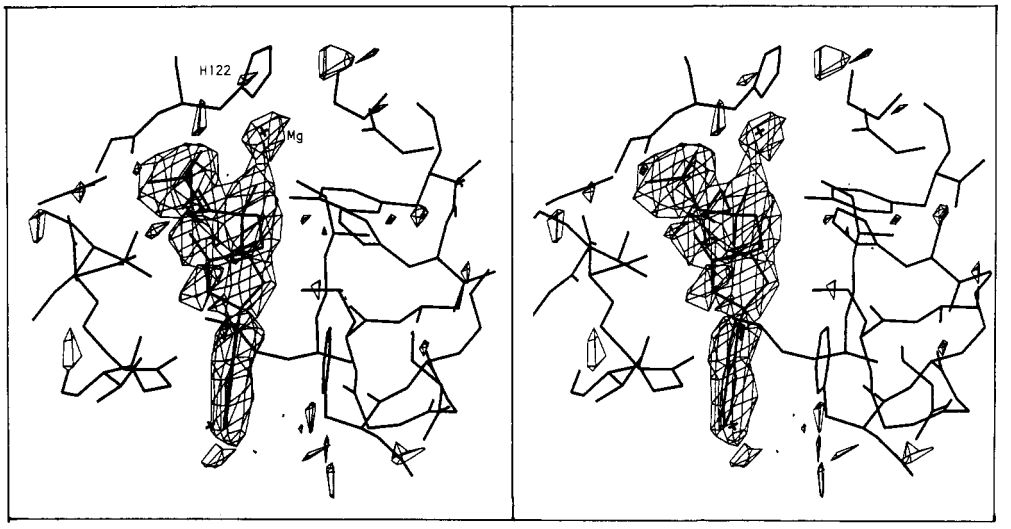

FIGURE 1: Electron density for ADP bound to NDP kinase. The $F_o - F_c$ map is calculated with ADP and the Mg^{2+} ion removed from the refined atomic coordinates and contoured at 3σ. Part of the active site of subunit B is shown with His 122 on top. The cross is Mg^{2+}. Drawn with FRODO (Jones, 1985).

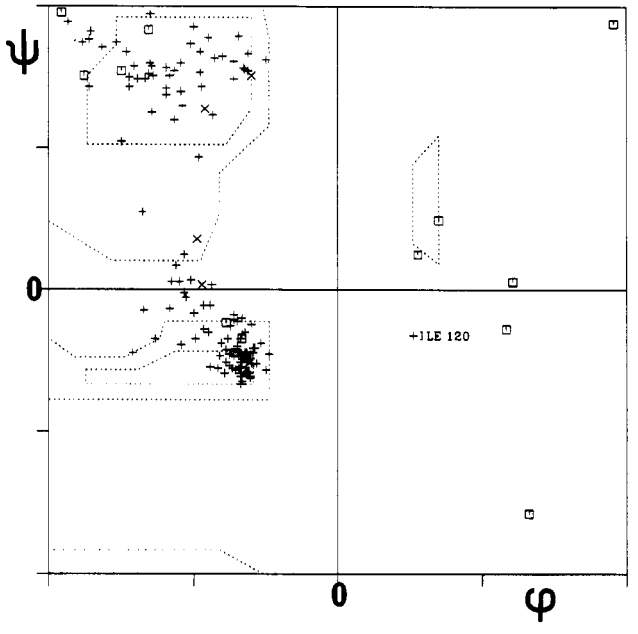

FIGURE 2: Ramachandran diagram for subunit B in form III: (□) Gly residues; (+) others.

157 water molecules. It has an *R*-factor of 0.19 at 2.2-Å resolution.

Quality of Models. The quality of the refined models of the NDP kinase subunit can be judged from data in Table 2 and from Ramachandran diagrams (Figure 2). Only one non-glycine residue is outside permitted regions of the diagram: Ile 120, located just before strand β_4. Its (ϕ, ψ) angles are near (60, –40) in all our models, and the electron density clearly shows the main-chain conformation to be unusual.

The RMS discrepancy between various models after least-squares superposition is another measure of their accuracy. For 148 Cα positions, the RMS distance between H122C and the wild type in form II is 0.24 Å (Figure 3a). Between wild-type forms I and II, it is 0.33 Å; between form II and subunit A of the ADP–Mg^{2+} complex (form III), it is 0.40 Å. The first two RMS values are compatible with an estimated error of 0.2 Å on Cα positions and with the dependence of the *R*-factor on resolution. The third value includes local conformation changes that are discussed below. In form III, the accuracy of atomic positions can also be judged from the RMS deviation from local 2-fold symmetry in the two independent subunits: it is 0.23 Å for the Cα and 0.52 Å for all protein atoms.

Mobility of the polypeptide chain can be estimated from the *B*-factors in Figure 3b. The free enzyme in form II has *B*-factors less than 20 $Å^2$ except for segments 57–65 and 139–151. Segment 57–65 is better ordered in the ADP–Mg^{2+} complex.

RESULTS

Structure of Wild-Type NDP Kinase. The overall structure of *Dictyostelium* NDP kinase is illustrated in Figure 4 for the ADP–Mg^{2+} complex. The molecule is a hexamer; it has dihedral 3-fold symmetry and forms a compact disk about 70 Å in diameter and 50 Å thick. The 3-fold axis defines a vertical direction common to all three crystal forms. Subunits related by the 3-fold axis form "horizontal" trimers; by 2-fold axes, "vertical" dimers. Thus, the hexamer has a "top" and a "bottom" trimer and three vertical dimers. In form III, top and bottom subunits are nonequivalent from a crystallographic point of view. Though they remain essentially identical, they are labeled A and B below.

Each 17-kDa subunit of the hexamer contains an α/β domain comprising residues 8–138. Residues at the N-terminus are disordered. The chain ends with an extended outer segment comprising residues 139–155. The central β-sheet of the α/β domain is antiparallel and four-stranded with strand order $\beta_2\beta_3\beta_1\beta_4$. The β-strands alternate along the sequence with α-helices. The β-sheet extends from one subunit to its partner in a dimer through vertical contacts between β_2 edge strands. Horizontal contacts within trimers involve helices α_1 and α_3 and a remarkable feature of the NDP kinase subunit, the Kpn loop (residues 99–118, between α_3 and β_4). Three Kpn loops come together near the 3-fold axis on the top of the disk; three others, on the bottom. The Kpn loop takes its name from the *killer of prune* (*K-pn*) mutation of *Drosophila* (Sturtevant, 1956), which has been shown to occur in the *awd* gene coding for NDP kinase (Biggs et al., 1988). *K-pn* substitutes a serine for the proline residue equivalent to Pro 100 in *Dictyostelium*, lowering the stability of the hexamer while keeping the enzymic activity intact (Lascu et al., 1992).

Whereas wild-type and H122C subunits in form II are identical within experimental error, significant changes are

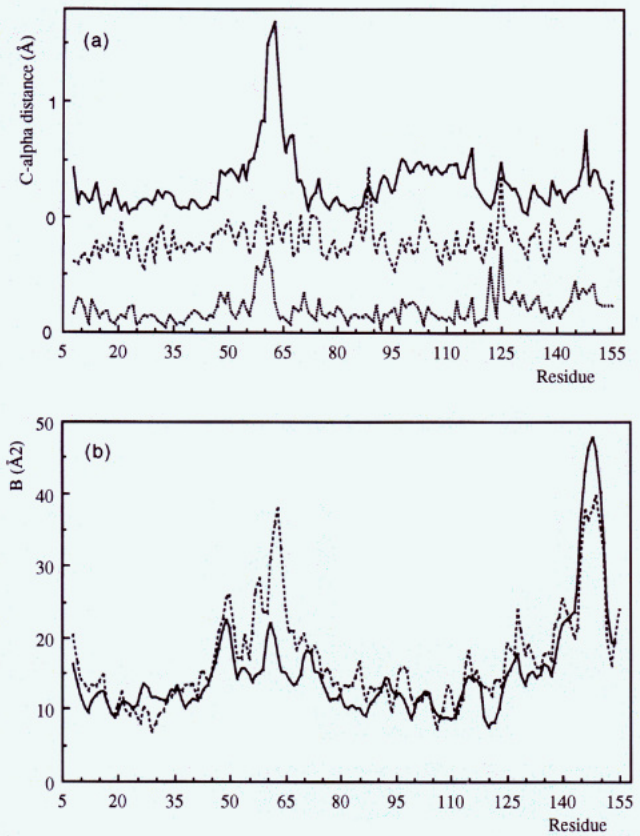

FIGURE 3: Main-chain movements in NDP kinase. (a) Distance between equivalent Cα positions after least-squares superposition of (dots) the H122C mutant and the wild type in form II, (dashes, shifted up by 0.5 Å) wild-type forms I and II, and (full line) form II and subunit A of the ADP–Mg^{2+} complex. (b) Temperature factors for main-chain atoms in the wild-type form II (dashes) and in subunit B of the ADP–Mg^{2+} complex (full line).

seen in the ADP–Mg^{2+} complex. As can be seen in Figure 3a, the polypeptide main chain moves by up to 2 Å at residues 59–65. These residues belong to the surface loop that connects helix α_A (residues 49–55) to α_2 (residues 65–73). This part of the polypeptide chain is less well ordered than average, and α_A was not recognized to be a helix in the original H122C structure. Yet, the movement of residues 59–65 is significant, and we shall see that it is directly related to the presence of the nucleotide.

ADP–Mg^{2+} Binding. ADP binding to *Dictyostelium* NDP kinase is described in Figures 4–6. The hexamer carries six binding sites about 40 Å apart. The sites are equivalent, and no site-to-site interaction is expected, consistent with Michaelian kinetics of the enzyme. However, crystal packing in the *R*3 crystal form brings nucleotides bound to B subunits in one hexamer almost in contact with A subunits of the hexamer just below. Differences in the nucleotide environment will be mentioned even though they almost certainly are crystal packing artifacts.

The nucleotide is bound with the base close to the protein surface and the pyrophosphate moiety near the imidazole of His 122 (Figure 5). It stretches parallel to strand β_4 which carries His 122, on the edge rather than against the face of the β-sheet, and it does not interact with the N-terminus of an α-helix. The adenosine moiety is in a cleft between helix α_2 and segment 116–119 of the polypeptide chain. This segment ends the Kpn loop just before strand β_4. Dihedral angles defining the nucleoside conformation are quoted in Table 3. The glycosidic bond is *anti* and the ribose pucker C3′-*endo* in subunit B and C2′-*exo* in subunit A.

FIGURE 4: Two orthogonal views of the NDP kinase hexamer: (a, top) view along the 3-fold axis; (b, bottom) view along a 2-fold axis. Drawn with program O (Prof. T. A. Jones, Uppsala).

ADP interactions are listed in Table 4. The adenine base makes no polar contact with the protein. It is stacked on Phe 64 from helix α_2 and caught between the phenyl group of Phe 64 on one side the Val 116 side chain and Gly 117 Cα on the other (Figure 6). Further on helix α_2, Leu 68 makes nonpolar contacts with the ribose ring. When the complex is superposed on the free enzyme, Phe 64 and helix α_2 as a whole are seen to move toward the Kpn loop by about 2 Å, closing the cleft onto the nucleoside. Table 3 shows that the base remains largely accessible to the solvent through the ring nitrogens N1 and N3 and the exocyclic amino group. These polar atoms are on the protein surface and interact with water molecules. Remarkably, the C-terminal residue Glu 155′ of a neighboring subunit in the trimer approaches the adenine base from outside. Glu 155′ is held in position by a H-bond from its NH to the side chain of Asp 115. Its δ-carboxylate group is within 4.5 Å of both N1 and N3, yet there appears to be only solvent-mediated interactions.

Unlike the base, the ribose is almost completely buried. Its hydroxyls in the 2′ and 3′ positions are involved in polar interactions: $O_{2'}$ with the ε-amino group of Lys 16 and $O_{3'}$ with the amide group of Asn 119. Whereas an amino group

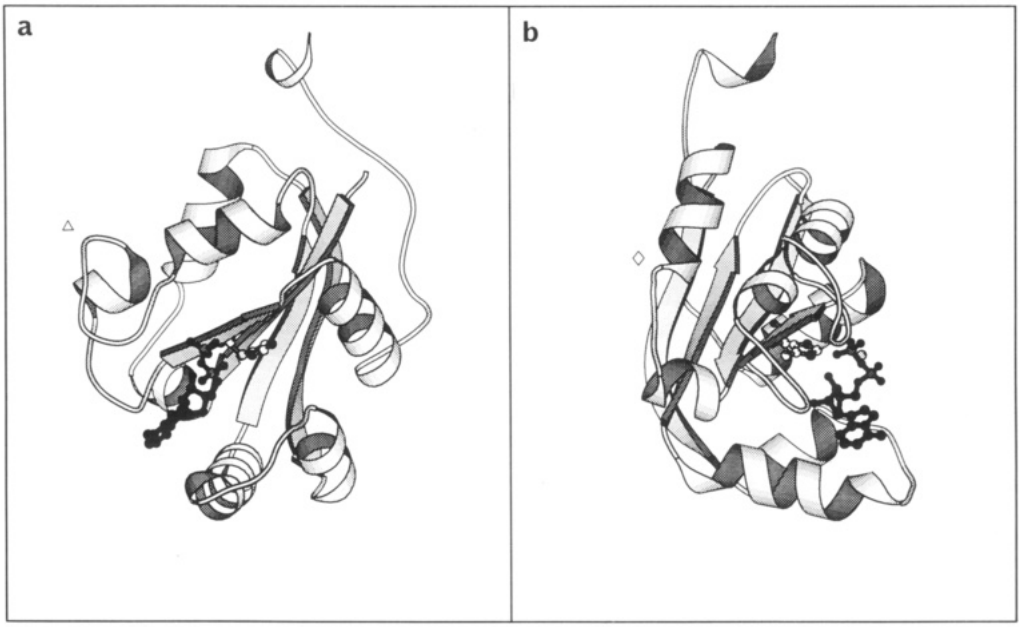

FIGURE 5: Two orthogonal views of ADP bound to a NDP kinase subunit: (a) view along the 3-fold axis (△); (b) view along a 2-fold axis (◇). ADP is in black. Strand β_4 is in front with His 122 in a ball-and-stick model. The bottom helices are α_A and α_2. The Kpn loop is near the 3-fold axis; it contains a turn of α-helix. Drawn with MOLSCRIPT (Kraulis, 1991).

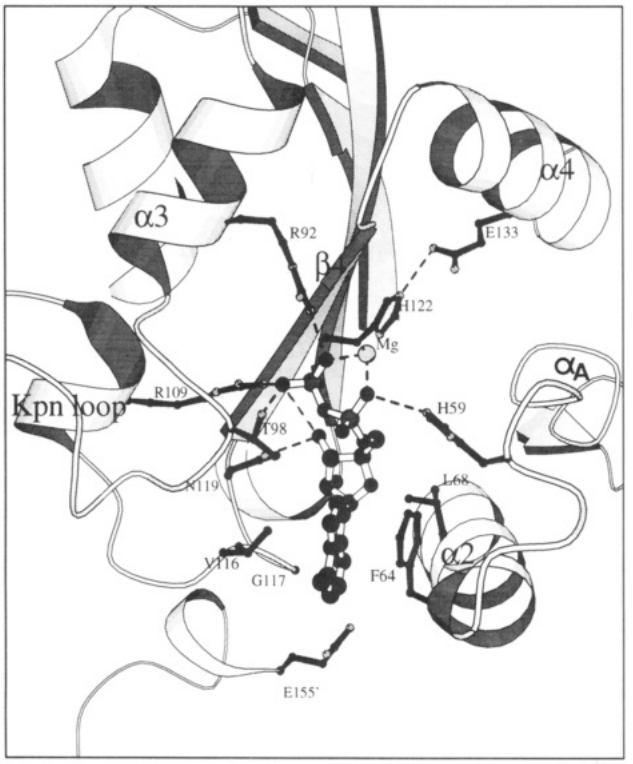

FIGURE 6: Nucleotide binding site. The orientation is close to that in Figure 5a: ADP in empty bonds, residues forming the site in full bonds, and N and O atoms in gray. Glu 155′ on the bottom is at the C-terminus of an adjacent subunit. Drawn with MOLSCRIPT (Kraulis, 1991).

can only donate H-bonds, an amide is both donor and acceptor. We chose to orient the Asn 119 amide so that its nitrogen donates an H-bond to $O_{3'}$ and its oxygen receives one from Lys 16. Then, $O_{3'}$ can be donor in an intramolecular H-bond with the β-phosphate which has an oxygen less than 3 Å from $O_{3'}$. The α-phosphate remains partly accessible to the solvent. It makes no direct interaction with the protein except possibly with His 59. As no phosphate oxygen is nearer than 3 Å, the interaction is probably weak. In contrast, the β-phosphate is buried deeper inside the protein, and it makes several

Table 3: Bound ADP Conformation and Accessibility to Solvent

	free ADP	subunit A	subunit B
dihedral angles			
glycosidic bond, χ		−142	−137
sugar pucker,[a] P		−16	20
accessible surface (Å^2)[b]			
base	198	88	89
ribose	142	1	2
α-phosphate	73	22	32
β-phosphate	104	5	9
total	517	116	132

[a] The pseudorotation angle P is defined as in Saenger (1984). [b] Solvent-accessible surface areas were calculated with the program ASA (Prof. A. Lesk, Cambridge) and a probe size of 1.4 Å. Free ADP is taken from subunit B.

electrostatic interactions with the guanidinium groups of Arg 92 and Arg 109 and also with the hydroxyl of Thr 98.

In subunit B, the electron density map locates a Mg^{2+} ion next to the pyrophosphate moiety of ADP. The metal ion is bound to the O_{11} and O_{21} atoms, bridging the α- and β-phosphates. No protein atom interacts with it, but four water molecules complete its coordination octahedron. All six metal–oxygen distances are in the 2.0–2.2-Å range expected for Mg^{2+}. In subunit A, the density is compatible with a Mg^{2+} ion bridging the α- and β-phosphates, but the bonds are longer and the metal ion was modeled as water.

His 122 and the Active Site. The environment of His 122 is described in Figure 7. His 122 is part of strand β_4 at the edge of the central β-sheet. Its side chain is *trans* to the amino group, with the imidazole ring lying flat on the main chain. It points toward the C-terminus of β_4 and into a cleft between helices α_A and α_4. The position of the imidazole ring is fixed by an H-bond from Nϵ to the carboxylate of Glu 133. This interaction cannot be made if the ring flips. The His 122 side-chain conformation is essentially the same with and without ADP as shown by the dihedral angles and distances to interacting groups (Table 5). In the complex, the nearest ADP atom is O_7 of the β-phosphate. The distance to Nδ is 4.7 Å, and a water molecule (water 46) bridges Nδ and O_7.

Table 4: ADP–Mg^{2+} Interactions

ADP	protein	distance (Å)[a] for subunit A	B
base			
nonpolar	Phe 64 ring	3.9	3.6
C_5	Cγ1 Val 116	3.9	3.4
N_3	Cα Gly 117	3.9	3.7
ribose			
nonpolar $O_{4'}$	Phe 64 ring	3.9	3.4
	Cδ2 Leu 68	3.2	3.2
polar			
$O_{2'}$	Nζ Lys 16	3.1	2.6
$O_{3'}$	Nδ Asn 119	2.8	2.9
	Nζ Lys 16	3.6	2.7
α-phosphate			
$O_{5'}$	Nε His 59	3.3	3.6
O_{11}	Nε His 59	3.9	3.0
	Mg^{2+}	2.9[b]	2.0
β-phosphate			
O_{21}	Nη2 Arg 92	3.2	2.9
	Mg^{2+}	2.8[b]	2.3
O_{22}	Nη2 Arg 109	3.0	2.7
	Oγ Thr 98	2.8	3.1
O_7	Nη1 Arg 109	3.5	2.8
	water 46		2.8

[a] Distances are quoted for both subunits in the asymmetric unit. In the case of nonpolar interactions, they refer to the shortest contact. [b] In subunit A, Mg^{2+} may be replaced with solvent.

Residues surrounding His 122 are Phe 12, His 55, Tyr 56, and Ser 124. His 55 has its imidazole group next to that of His 122. The two rings are approximately orthogonal and in van der Waals contact, yet they make no polar interaction when oriented as shown in Figure 7. Rather, His 55 Nδ receives an H-bond from the indole NH of Trp 137, only 2.7 Å away. The Phe 12 and Tyr 56 rings are also orthogonal to the His 122 imidazole and in van der Waals contact with it. In addition, the Tyr 56 phenol group H-bonds to the water molecule mentioned above (water 46).

The side-chain contact between His 122 and Ser 124 is to be expected for residues two apart on the same β-strand β_4. It involves no polar interaction, Ser 124 Oγ being 4.5 Å from His 122 Nε. Both groups are engaged in H-bonds with the carboxylate of Glu 133, Oγ perhaps also with the main-chain NH of Phe 12 on the adjacent strand β_1. If Ile 120 were part of strand β_4, it should also be in contact with His 122, and its side chain would block access to the imidazole group. Instead, Ile 120 adopts nonstandard φ, ψ angles (Figure 2) which place its side chain on the opposite face of the β-strand.

DISCUSSION

The ADP Binding Site. Nucleotide binding sites have been characterized in many protein structures. They are often associated with the βαβ structural motif ("Rossmann fold"), first identified in NAD-dependent dehydrogenases (Rossmann et al., 1975). The nucleotide binds at the N-terminal end of the α-helix, which has free NH groups giving H-bonds to the phosphate group. In addition, the helix dipole may contribute to the binding energy. The βαβ motif is found in many phosphokinases and also in GTP binding proteins such as $p21^{ras}$ and EF-Tu (Saraste et al., 1991; Schulz, 1992). These proteins belong to the α/β protein class with a parallel β-sheet, and their sequence includes a glycine-rich loop, the "P-loop", where the glycines make NH to phosphate bonds sterically feasible. In the cAMP-dependent protein kinase, ATP also binds to main-chain NH's and to lysines (Bossemeyer et al., 1993; Zheng et al., 1993). Again, a glycine-rich sequence is involved, but it forms a β-hairpin quite unlike the βαβ or P-loop structural motifs.

NDP kinase has no Rossmann fold or P-loop, and the only glycine at the nucleotide binding site is Gly 117, in contact with the base rather than with phosphates. The role of two other glycine residues has been tested by site-directed mutagenesis of the *Myxococcus xanthus* enzyme (Muñoz-Dorado et al., 1993). The G21V and G91V substitutions led to a loss of activity. Gly 21 is equivalent to Gly 26 in *Dictyostelium*. It is remote (20 Å) from the nucleotide binding site described here and at the dimer interface, which may be the reason for the loss of activity. Gly 91, equivalent to our Gly 96, is nearer but not in direct contact either. Gly 96 has (ϕ, ψ) angles of (115, −150) which are forbidden to other residues, and the substitution may perturb the structure.

The four-stranded antiparallel β-sheet found in NDP kinase is a recurrent motif in nucleotide binding proteins, distinct from the Rossmann fold (Dumas et al., 1992). It is present in the allosteric domain of ATCase (Gouaux et al., 1990), in the U1 small ribonucleoprotein A (Nagai et al., 1990), and, in a modified version, in the recently determined structure of glutathione synthetase (Yamaguchi et al., 1993). Whereas similarity with the ATCase allosteric domain extends to the mode of dimer association, the mode of binding is different (Figure 8). After the β-sheets are superposed, the phosphates are only 6 Å apart, yet the riboses and bases point to opposite directions. In ATCase, the nucleotide lies on the open face of the β-sheet. In NDP kinase, this face is partly covered by α_A, α_2, and α_4, and ADP binds to the edge of the β-sheet. It interacts mostly with α_2 and the Kpn loop, a unique feature of this protein.

The nucleotide binding site described here is original in other ways. There is no polar interaction with main-chain groups, only with side chains: two arginines and a threonine for the pyrophosphate and a lysine and an asparagine for the ribose. The lack of polar interactions to the base is not unusual for adenine. It fits with kinetic data: NDP kinase shows very little specificity toward the nature of the base (Parks & Agarwal, 1973). As polar atoms remain in contact with the solvent at the protein surface, any aromatic compound should be able to fill the site between Phe 64 and Val 116. Phe 64 is strictly conserved in all known NDP kinase sequences [a recent alignment can be found in Shimada et al. (1993)], whereas Val 116 is sometimes replaced with other branched side chains. Gly 117 is also conserved. Its Cα is in contact with the base, and a side chain at this position would hinder binding.

Hexamers are rare among phosphate-transfer proteins. The quaternary structure of NDP kinase plays no obvious part in nucleotide binding. We noted, however, that the C-terminal Glu 155 of an adjacent subunit makes water-mediated interactions with the adenine base. These interactions could in principle distinguish between purines and pyrimidines. Glu 155 is conserved in NDP kinase sequences, even though the C-terminal segment 139–155 shows high variability. The segment is fully exposed on the surface of the hexamer and rather mobile as shown by high *B*-factors (Figure 3b), though the C-terminus itself is held in place by intersubunit contacts. Further crystallographic and biochemical experiments should assess its role.

NDP kinase accepts deoxynucleotides as well as nucleotides as substrates. Still, the 2′- and the 3′-hydroxyls of the ribose make specific interactions with Lys 16 and Asn 119, two strictly conserved residues. In these interactions, the sugar hydroxyls act as H-bond acceptors, while in many nucleotide binding proteins, there is an aspartate where we find Asn 119. Its carboxylate receives a H-bond from either or both hydroxyls.

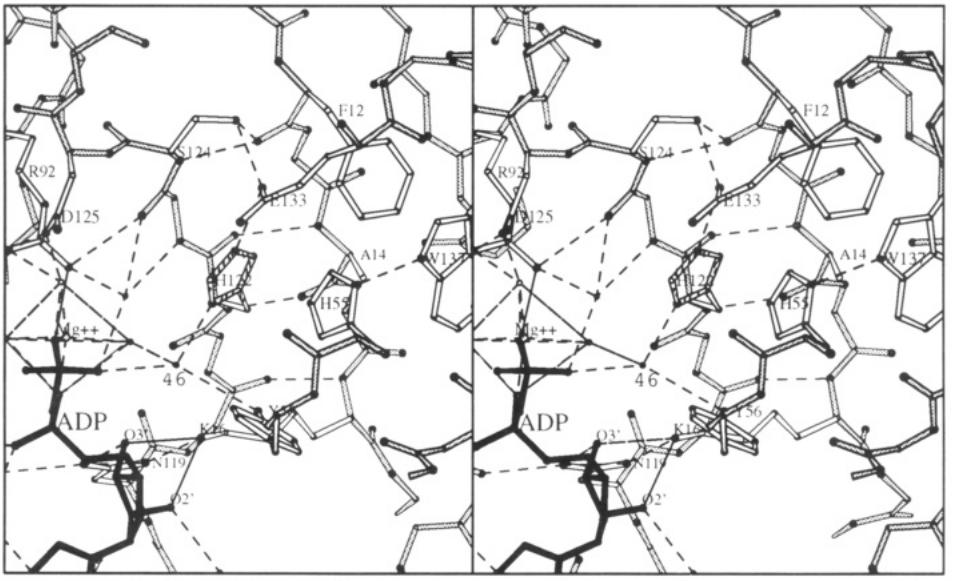

FIGURE 7: NDP kinase active site: stereo pair of subunit B. The environment of His 122 includes side chains of neighboring residues (empty bonds), the ribose and pyrophosphate part of ADP (full bonds), the Mg^{2+} ion, and a number of water molecules (dots). N and O atoms are shaded. Drawn with MOLSCRIPT (Kraulis, 1991).

Table 5: His 122 Conformation

	form II (no ADP)	form III	
		A	B
dihedral angles			
χ_1	168	163	163
χ_2	94	87	80
distances (Å)			
Nϵ–Glu 133 (Oϵ2)	2.9	2.8	2.8
Nδ–Wat 46			2.5

The bonding pattern observed here requires the sugar ring to be in the C3′-*endo* conformation, which is favorable with ribose but less so with deoxyribose. Whether deoxynucleotides make compensating interactions remains to be determined.

Guanidinium and hydroxyl groups are commonly involved in binding phosphate groups. Here, the β-phosphate interacts with three strictly conserved protein residues: Arg 92, Thr 98, and Arg 109. Since a Mg^{2+} ion bridges the two phosphate groups, two guanidinium groups is more than required for compensating the negative charge carried by the pyrophosphate (probably –3 above pH 7). One of the two arginines, Arg 92 probably, should also interact with the γ-phosphate of ATP when present. Another basic side chain is in the immediate vicinity of the α-phosphate, that of His 59. As this residue is replaced with a leucine in many NDP kinase sequences, no functional role can be attributed to the imidazole group.

A Model for Phosphate Transfer to His 122. In the ADP–Mg^{2+} complex, the pyrophosphate moiety of ADP does not interact directly with His 122. The shortest distance to the imidazole is 4.7 Å, which leaves room for the γ-phosphate of ATP. The geometry observed in the ADP–Mg^{2+} complex is well suited for the additional phosphate to be transferred onto His 122. We noted that a water molecule bridges the β-phosphate to the imidazole Nδ. In Figure 9, we substituted Pγ for this water molecule, made its two H-bonds into axial bonds, and added three equatorial oxygens. The resulting construction resembles the putative pentacoordinated intermediate during transfer of the γ-phosphate with inversion of configuration. The two H-bonds of the water molecule are only slightly longer than the partial covalent bonds they represent. It should be recalled that, in the mechanism represented by eq 1, the γ-phosphate configuration is inverted twice during catalysis by NDP kinase, once upon His 122 phosphorylation by XTP, and then again upon its dephosphorylation by YDP. As a result, its configuration is the same in the product YTP as in the substrate XTP (Rex Sheu et al., 1979). The transfer is fully reversible, the triphosphates and the phosphohistidine having very similar free energies of hydrolysis.

Basic assumptions of our model are that the histidine is phosphorylated on Nδ rather than on Nϵ and that it does not change conformation during phosphate transfer. These assumptions are supported by the imidazole interaction with Glu 133, which implies that Nϵ is protonated and not available for phosphorylation. In contrast, Nδ should be deprotonated at pH 7–9 where the enzyme has maximum activity (data not shown) and therefore is capable to act as a nucleophile attacking Pγ in its assumed position.

Polar interactions with equatorial oxygens may stabilize the pentacoordinated intermediate and contribute to catalysis. Two conserved protein side chains are poised to do so: those of Lys 16, which also interacts with the ribose, and of Tyr 56. We exclude His 55 from the mechanism in spite of its immediate vicinity to His 122. It is replaced with a Phe in *Myxococcus* NDP kinase, and we have evidence that its substitution with Ala or Gln has no major effect on the catalytic activity of the *Dictyostelium* enzyme.

In contrast to His 55, Ser 124 is fully conserved. Its location on strand β_4 does not allow its side chain to interact with the phosphate group being transferred. It could, however, do so after His 122 is phosphorylated, provided the H-bond to Glu 133 breaks and the imidazole group flips over. While these events may be very slow on the time scale of the catalytic cycle (less than 1 ms), they could conceivably lead to phosphorylation of the serine, which would be essentially irreversible unlike histidine phosphorylation. Phosphohistidine is acid labile. The formation of an acid-stable phosphorylated derivative has been described with the *Myxococcus* enzyme incubated with ATP and EDTA (Muñoz-Dorado et al., 1993). It was abolished after the active site histidine was mutated, and the phosphorylated residue was identified as serine.

Comparison with Other Histidine Kinases. Though less ubiquitous than Ser/Thr phosphorylation, histidine phos-

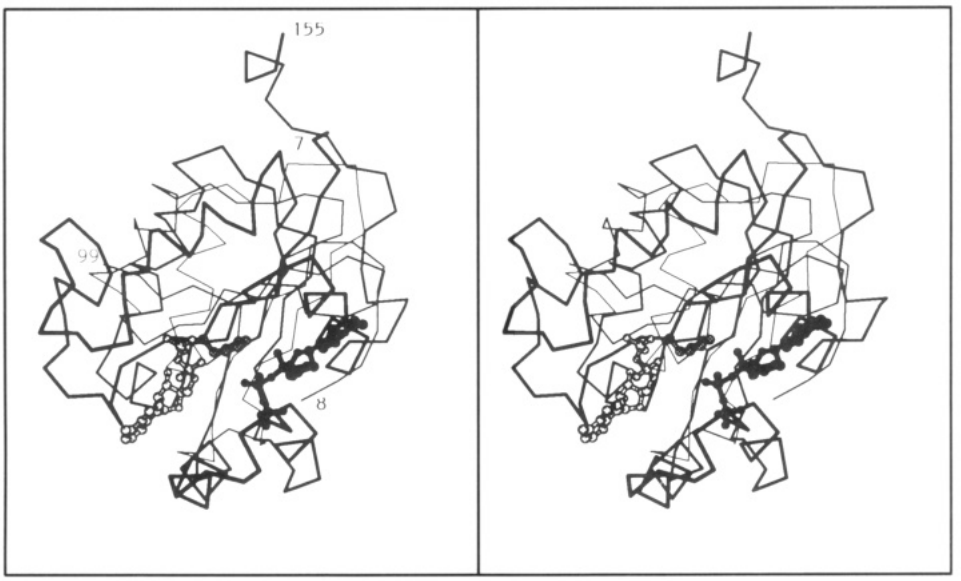

FIGURE 8: Nucleotide binding to NDP kinase and to the allosteric domain of *E. coli* ATCase: stereo pair of the NDP kinase subunit superimposed onto residues 8–99 of the regulatory chain of *E. coli* ATCase (Gouaux et al., 1990) by fitting equivalent β-strands β_1–β_4. NDP kinase is in thick lines with His 122 and bound ADP in gray, and ATCase is in thin lines with bound ATP in black. Drawn with MOLSCRIPT (Kraulis, 1991).

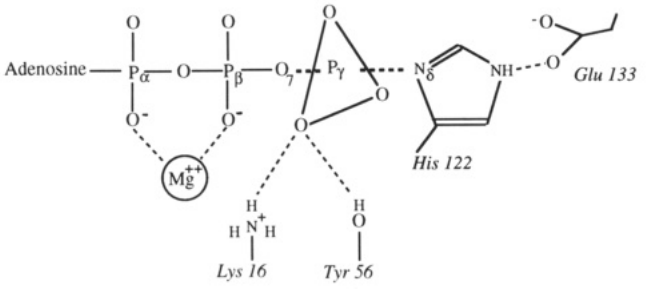

FIGURE 9: Transition state for phosphate transfer. The γ-phosphate of the nucleoside triphosphate substrate is transferred onto the unprotonated Nδ atom of His 122 via a pentacoordinated intermediate, with inversion of its configuration. One of the three equatorial oxygen atoms is in position to H-bond with Lys 16 and Tyr 56. Arg 92 and a second metal ion may interact with the other two oxygens. The transfer is fully reversible, and the same intermediate occurs upon phosphorylation of the nucleoside diphosphate substrate completing the catalytic cycle.

phorylation is an essential part of several enzymic mechanisms. In bacteria, it has major physiological functions reviewed by Stock et al. (1989, 1990): chemotaxis and the regulation of nitrogen and phosphate uptake, for instance. One of the best characterized processes in this category is sugar transport. The phosphoenolpyruvate:glucose phosphotransferase system [PTS, reviewed by Meadow et al. (1990)] carries the phosphate group of phosphoenolpyruvate onto a sugar hydroxyl via a series of transport proteins, all phosphorylated on histidines. Three-dimensional structures are known for several components of the PTS system, the small protein HPr (Wittekind et al., 1990; Herzberg et al., 1992), and two related protein domains called IIA^{Glc} and III^{Glc} (Liao et al., 1991; Worthylake et al., 1991; Hurley et al., 1993).

HPr is phosphorylated on the Nδ atom of His 15. It binds to domain IIA and transfers its phosphate onto the Nϵ atom of His 83 of IIA. A model-built HPr–IIA complex suggests that the transfer requires no change in their conformation (Herzberg, 1992). Though Jia et al. (1993) make the opposite assumption, NMR data on a related complex support this hypothesis (Chen et al., 1993). HPr is built around a four-stranded antiparallel β-sheet like NDP kinase, but the topology is different and the phosphorylated His 15 is at the N-terminus of an α-helix, not on a β-strand. In proteins IIA^{Glc} and III^{Glc}, which are essentially pure β-sheet, the phosphorylated histidine is C-terminal to a central β-strand and in close contact with another histidine which may stabilize its phosphorylated form.

A pair of histidine residues also constitute the active site of phosphoglycerate mutase and of several related enzymes reviewed by Fothergill-Gilmore and Watson (1989). Phosphoglycerate mutase shuttles a phosphate group between C_2 and C_3 of phosphoglycerate via an intermediate where His 8 is phosphorylated. Whereas His 8 is C-terminal to a β-strand like its counterpart in domain IIA, the geometry of the active site is different and the role of the adjacent histidine is probably unrelated (Liao et al., 1991). As for His 55 of *Dictyostelium* NDP kinase, it seems to be unessential in catalysis even though its imidazole is in contact with His 122. Thus, there appears at this stage to be little in common among these proteins in terms of three-dimensional structure and function beyond using phosphohistidine as an energy-rich phosphate donor.

NOTE ADDED IN PROOF

The X-ray structure of *M. xanthus* NDP kinase has recently been solved (Williams et al., 1993). Dr. R. L. Williams (Cambridge, U.K.) has kindly made atomic coordinates available to us prior to deposition. The bacterial protein is a tetramer. The polypeptide chain fold, the mode of dimer association, and the ADP binding site are remarkably similar in the two proteins in spite of a relatively low sequence identity and of different quaternary structures.

ACKNOWLEDGMENT

We are grateful to Dr. M. L. Lacombe for the NDP kinase expression vector, to Dr. P. Marlière and V. Wallet for producing seleniated protein, and to Prof. R. Fourme, Prof. J. P. Benoît, and the staff of LURE (Orsay) for making station W32 on the wiggler line of LURE-DCI available to us.

REFERENCES

Adman, E. T., Sieker, L. C., & Jensen, L. H. (1973) *J. Biol. Chem. 248*, 3987–3996

Biggs, J., Tripoulas, N., Hersperger, E., Dearolf, C. R., & Shearn, A. (1988) *Genes Dev. 2*, 1333–1343.

Bossemeyer, D., Engh, R. A., Kinzel, V., Poinstingl, H., & Huber, R. (1993) *EMBO J. 12*, 849–859.
Brünger, A. T., Kuriyan, J., & Karplus, M. (1987) *Science 235*, 458–460.
Chen, Y., Reizer, J., Saier, M. H., Fairbrother, W. J., & Wright, P. E. (1993) *Biochemistry 32*, 32–37.
Dumas, C., Lebras, G., Wallet, V., Lacombe, M.-L., Véron, M., & Janin, J. (1991) *J. Mol. Biol. 217*, 239–240.
Dumas, C., Lascu, I., Moréra, S., Glaser, P., Fourme, R., Wallet, V., Lacombe, M. L., & Janin, J. (1992) *EMBO J. 11*, 3203–3208.
Fothergill-Gilmore, L. A., & Watson, H. C. (1989) *Adv. Enzymol. 62*, 227–313.
Gilles, A. M., Presecan, E., Vonica, A., & Lascu, I. (1991) *J. Biol. Chem. 266*, 8784–8789.
Gouaux, J. E., Stevens, R. C., & Lipscomb, W. N. (1990) *Biochemistry 29*, 7702–7715.
Hendrickson, W. A. (1985) in *Methods in Enzymology, Diffraction Methods for Biological Molecules, Part B* (Wyckoff, H. W., Hirs, C. H. W., & Timasheff, S. N., Eds.) Vol. 115, pp 252–270, Academic Press, London.
Hendrickson, W. A., Horton, J. R., & LeMaster, D. M. (1990) *EMBO J. 9*, 1665–1672.
Herzberg, O. (1992) *J. Biol. Chem. 267*, 24819–24823.
Herzberg, O., Reddy, P., Sutrina, S., Saier, M. H., Jr., Reizer, J., & Kapadia, G. (1992) *Proc. Natl. Acad. Sci. U.S.A. 89*, 2499–2503.
Hurley, J. H., Faber, H. R., Worthylake, D., Meadow, N. D., Roseman, S., Pettigrew, D. W., & Remington, S. J. (1993) *Science 259*, 673–677.
Jia, Z., Vandonselaar, M., Quail, W., & Delbaere, L. T. J. (1993) *Nature 361*, 94–97.
Jones, T. A. (1985) in *Methods in Enzymology, Diffraction Methods for Biological Molecules, Part B* (Wyckoff, H. W., Hirs, C. H. W., & Timasheff, S. N., Eds.) Vol. 115, pp 157–170, Academic Press, London.
Kraulis, P. (1991) *J. Appl. Crystallogr., 24*, 946–950.
Lacombe, M. L., Wallet, V., Troll, H., & Véron, M. (1990) *J. Biol. Chem. 265*, 10012–10018.
Lascu, I., Chaffotte, A., Limbourg-Bouchon, B., & Véron, M. (1992) *J. Biol. Chem. 267*, 12775–12781.
Leslie, A. G. W., Brick, P., & Wonacott, A. T. (1986) *Daresbury Lab. Inf. Q. Protein Crystallogr. 18*, 33–39.
Liao, D. I., Kapadia, G., Reddy, P., Saier, M. H., Jr., Reizer, J., & Herzberg, O. (1991) *Biochemistry 30*, 9583–9594.
Meadow, N. D., Fox, D. K., & Roseman, S. (1990) *Annu. Rev. Biochem. 59*, 497–542.
Muñoz-Dorado, J., Almaula, N., Inouye, S., & Inouye, M. (1993) *J. Bacteriol. 175*, 117–1181.
Nagai, K., Oubridge, C., Jessen, T. H., Li, J., & Evans, P. R. E. (1990) *Nature 348*, 515–520.
Parks, R. E., Jr., & Agarwal, R. P. (1973) *Enzymes 8*, 307–334.
Rex Sheu, K. F., Richard, J. P., & Frey, P. A. (1979) *Biochemistry 18*, 5548–5556.
Rosengard, A. M., Krutzsch, H. C., Shearn, A., Biggs, J. R., Barker, E., Margulies, I. M. K., King, C. R., Liotta, L. A., & Steeg, P. S. (1989) *Nature 342*, 177–180.
Rossmann, M. G., Liljas, A., Bränden, C. I., & Banaszak, L. J. (1975) *Enzymes 11*, 61–102.
Saenger, W. (1984) *Principles of Nucleic Acid Structure*, Springer Verlag, New York.
Saraste, M., Sibbald, P. R., & Wittinghofer, A. (1991) *Trends Biochem. Sci. 15*, 430–434.
Schulz, G. E. (1992) *Curr. Opin. Struct. Biol. 2*, 61–67.
Schulz, G. E., Schiltz, E., Tomasselli, A. G., Frank, R., Brune, M., Wittinghofer, A., & Schirmer, R. H. (1986) *Eur. J. Biochem. 161*, 127–132.
Shimada, N., Ishikawa, N., Munakata, Y., Toda, T., Watanabe, K., & Kimura, N. (1993) *J. Biol. Chem. 268*, 2583–2589.
Stock, J. B., Ninfa, A. J., & Stock, A. M. (1989) *Microbiol. Rev. 53*, 450–490.
Stock, J. B., Stock, A. M., & Mottonen, J. M. (1990) *Nature 344*, 395–400.
Sturtevant, A. H. (1956) *Genetics 41*, 118–123.
Wallet, V., Mutzel, R., Troll, H., Barzu, O., Wurster, B., Véron, M., & Lacombe, M.-L. (1990) *J. Natl. Cancer Inst. 82*, 1199–1202.
Williams, R. L., Oren, D. A., Munoz-Dorado, J., Inouye, S., Inouye, M., & Arnold, E. (1993) *J. Mol. Biol. 234*, 1230–1247.
Wittekind, M. G., Reizer, J., & Klevit, R. E. (1990) *Biochemistry 29*, 7191–7200.
Worthylake, D., Meadow, N. D., Roseman, S., Liao, D. I., Herzberg, O., & Remington, S. J. (1991) *Proc. Natl. Acad. Sci. U.S.A. 88*, 10382–10386.
Yamaguchi, H., Kato, H., Hata, Y., Nishioka, T., Kimura, A., Oda, J., & Katsube, Y. (1993) *J. Mol. Biol. 229*, 1083–1100.
Zheng, J., Knighton, D. R., Ten Eyck, L. F., Karlsson, R., Xuong, N., Taylor, S. S., & Sowadski, J. M. (1993) *Biochemistry 32*, 2154–2161.